Horizontal Redistribution of Two Fluid Phases in a Porous Medium: Experimental Investigations

Tim Feuring · Jürgen Braun · Barend Linders · Gerhard Bisch · S. Majid Hassanizadeh · Jennifer Niessner

Abstract Classical models for flow and transport processes in porous media employ the so-called extended Darcy's Law. Originally, it was proposed empirically for one-dimensional isothermal flow of an incompressible fluid in a rigid, homogeneous, and isotropic porous medium. Nowadays, the extended Darcy's Law is used for highly complex situations like non-isothermal, multi-phase and multi-component flow and transport, without introducing any additional driving forces. In this work, an alternative approach by Hassanizadeh and Gray identifying additional driving forces were tested in an experimental setup for horizontal redistribution of two fluid phases with an initial saturation discontinuity. Analytical and numerical solutions based on traditional models predict that the saturation discontinuity will

T. Feuring (✉)
CDM Smith Consult GmbH, Motorstrasse 5, 70499 Stuttgart, Germany
e-mail: tim.feuring@gmail.com

J. Braun
Research Facility for Subsurface Remediation (VEGAS), University of Stuttgart, Pfaffenwaldring 61, 70569 Stuttgart, Germany
e-mail: juergen.braun@iws.uni-stuttgart.de

B. Linders
Department of Water, Government of Western Australia, Perth, WA 6000, Australia
e-mail: barendlinders@gmail.com

G. Bisch
ARCADIS Deutschland GmbH, Griesbachstrasse 10, 76185 Karlsruhe, Germany
e-mail: g.bisch@arcadis.de

S. M. Hassanizadeh
Department of Earth Sciences, Utrecht University, Budapestlaan 4, 3584 CD Utrecht, The Netherlands
e-mail: S.M.Hassanizadeh@uu.nl

J. Niessner
Chair of Technical Physics and Fluid Mechanics, Heilbronn University, Max-Planck-Str. 39, 74081 Heilbronn, Germany
e-mail: Jennifer.Niessner@hs-Heilbronn.de

persist, but a uniform saturation distribution will be established in each subdomain after an infinite amount of time. The pressure field, however, is predicted to be continuous throughout the domain at all times and is expected to become uniform when there is no flow. In our experiments, we also find that the saturation discontinuity persists. But, gradients in both saturation and pressure remain in both subdomains even when the flow of fluids stops. This indicates that the identified additional driving forces present in the truly extended Darcy's Law are potentially significant.

Keywords Validity of Darcy's Law · Additional driving forces · Two-phase flow · Horizontal redistribution

1 Introduction

1.1 Motivation

The understanding of fluid flow and transport processes in porous media is very important for many applications in science and technology. An application in geology is the storage of carbon dioxide in deep geological formations. An example for a technical porous medium is the Polymer Electrolyte Membrane Fuel Cell, where a profound understanding of the involved flow and transport processes is needed for the design of an effective and powerful power supply.

A special case of flow in porous media is the horizontal redistribution of two fluid phases. In the vadose zone, this process is relevant, e.g., in agriculture, where the understanding of the horizontal spreading of water is important for the optimal irrigation of crops, especially in arid zones.

The problem of horizontal redistribution of water in soil was formulated and investigated mathematically by Philip (1991). It consists of an initial saturation discontinuity in an infinitely long, horizontal, one-dimensional, and homogeneous porous medium leading to two adjacent draining and imbibing subdomains. Due to its simplicity, the setup provides a suitable system for investigating driving forces for flow and testing the validity of the extended Darcy's Law. Despite its simplicity, the practical realization of this setup is challenging, both numerically and experimentally, because of the discontinuity in saturation.

1.2 Current Approaches to Modeling Horizontal Redistribution

To model the water redistribution problem, Philip (1991) used the flow equation by Richards (1931) for unsaturated flow in its one-dimensional horizontal form for isotropic homogeneous soils. Different capillary pressure-saturation curves were used for drainage and imbibition to account for capillary hysteresis. Similarity solutions were obtained for this system of equations. Recently, Pop et al. (2009) modeled the redistribution problem following the thermodynamically based approach of Hassanizadeh and Gray (1990). They used the traditional Darcy's Law but included a balance equation for fluid-fluid-specific interfacial area. Additionally, capillary hysteresis was accounted for by replacing the capillary pressure-saturation function by a capillary pressure-saturation-specific interfacial area surface, as suggested by Hassanizadeh and Gray (1993a). In another approach, Marshall (2009) divided the system into draining and imbibing subdomains coupled by an interface condition accounting for the mass conservation, continuity of capillary pressure and the saturation jump. The set of balance

equations was the same as in Pop et al. (2009). For the specific interfacial area, a bi-quadratic function as in Joekar-Niasar et al. (2008) is used. All solutions show a persisting saturation jump at the drainage-imbibition interface and continuity of capillary pressure across the interface. According to all numerical investigations, the system approaches a constant saturation and pressure distribution in both subdomains.

1.3 Purpose of this Work

The solutions discussed above all rely on theoretical models and have not been confirmed experimentally yet. The goal of this work is to close this gap and investigate horizontal redistribution using a setup similar to the one described in Philip (1991) and to investigate the following two issues: (1) Will a saturation discontinuity persist at the drainage-imbibition interface? (2) Will uniform saturations and pressures be established in both subdomains, after the flow of fluids ceases?

In Sect. 2, the classical and the thermodynamically based approaches for describing two-phase flow are explained. Next, in Sect. 3, the materials and methods used for conducting the experiments are introduced. In Sect. 4, results of experiments are presented and discussed. Finally, in Sect. 5, a summary and conclusions are given.

2 Classical Versus Thermodynamically Based Description

2.1 The Classical Approach

The classical approach describing isothermal two-phase flow in an incompressible porous medium employs continuity equations (Eq. (1)) and Darcy's Law (Eq. (2)) for each phase α, the wetting phase (w), and the non-wetting phase (n). These are complemented with the condition that the two fluid phases completely fill the pore space (Eq. 3), and a definition of a macro-scale capillary pressure (Eq. 4) (Helmig (1997)).

$$\varphi \frac{\partial S_\alpha}{\partial t} + \nabla \cdot \underline{v}_\alpha = Q_\alpha; \alpha = \text{w, n} \tag{1}$$

$$\underline{v}_\alpha = -\frac{k_{\text{r}\alpha} \underline{\underline{K}}}{\mu_\text{w}} \left(\nabla p_\alpha - \rho_\alpha \underline{g} \right) \tag{2}$$

$$S_\text{w} + S_\text{n} = 1 \tag{3}$$

$$p_\text{n} - p_\text{w} = p_\text{c}(S_\text{w}). \tag{4}$$

In these equations, φ is porosity, S_α is saturation, $\underline{v}_\alpha$ is Darcy velocity, Q_α is a source or sink term, $k_{\text{r}\alpha}$ is the relative permeability, μ_α is the viscosity, p_α is pressure, and ρ_α is the density of phase α. The tensor $\underline{\underline{K}}$ denotes the intrinsic permeability, $\underline{g}$ is gravity, and p_c is capillary pressure. Note that p_c and $k_{\text{r}\alpha}$ are functions of S_w.

As mentioned earlier, this extended Darcy's Law has basically the same form as the original equation introduced by Darcy (1856).

The coexistence of the phases is accounted for only using indices for the phases and introducing the relative permeability $k_{\text{r}\alpha}$, a scaling factor accounting for the reduction of permeability to a phase due to the presence of the other phase. The gradients in phase pressure and gravity are still the only driving forces for flow.

According to these classical equations for the redistribution problem, the initial saturation discontinuity will decrease and the system will approach constant saturation and capillary

pressure in both draining and imbibing subdomain. A persisting saturation discontinuity at the drainage-imbibition interface can only be realized using a hysteretic capillary pressure-saturation relationship. In practice, this means that a different $p_c(S_w)$ curve should be given for each subdomain.

2.2 A Thermodynamically Based Approach

Hassanizadeh and Gray (1990) developed a unified approach based on rational thermodynamics formulating balance equations not only for the solid and fluid phases but also for the phase interfaces and common lines, where all phases meet. In Hassanizadeh and Gray (1993b), the momentum balance equations were simplified, in order to obtain the following Darcy-type equations for the velocity of fluid phases, $\underline{v}_{\alpha,s}$

$$\varphi S_w \underline{v}_{w,s} = -\frac{S_w^2 \underline{K}_w}{\mu_w} [\left(\nabla p_w - \rho_w \underline{g} \right) + \frac{\lambda_{wn}}{a_{wn}} \nabla a_{wn} + \frac{\Omega_w}{S_w} \nabla S_w],$$ (5)

$$\varphi S_n \underline{v}_{n,s} = -\frac{S_n^2 \underline{K}_n}{\mu_n} [\left(\nabla p_n - \rho_n \underline{g} \right) - \frac{\lambda_{nw}}{a_{wn}} \nabla a_{wn} + \frac{\Omega_n}{S_n} \nabla S_w].$$ (6)

Here, $v_{\alpha,s}$ is the average pore velocity of the α-phase with respect to the solid phase, a_{wn} is the specific fluid-fluid interfacial area, $\underline{K}_\alpha$ is the permeability of phase α, Ω_α, and $\lambda_{\alpha\beta}$ are material parameters. In these balance equations, more driving forces are present than in the extended Darcy's Law.

Consider the case of no flow, $v_{\alpha,s} = 0$. Using the classical approach (see Eq. 2) this directly implies $\nabla p_\alpha = 0$, or $p_\alpha = $ const. for a horizontal system. But for the thermodynamically based model, Eqs. 5 and 6 do not imply a constant p_α. In fact it is possible to have $\nabla p_\alpha \neq 0$ that can be balanced by $\nabla a_{w,n}$ and/or ∇S_α. As mentioned above, the purpose of our experiment is to test whether the pressure gradients persist in the fluids after the flow ceases.
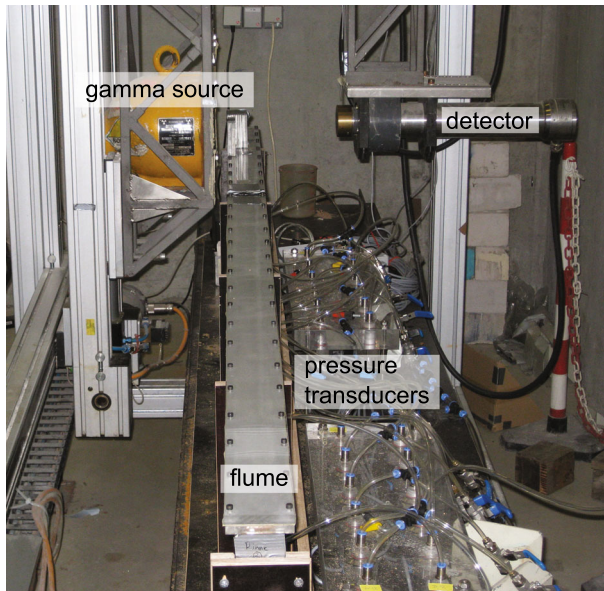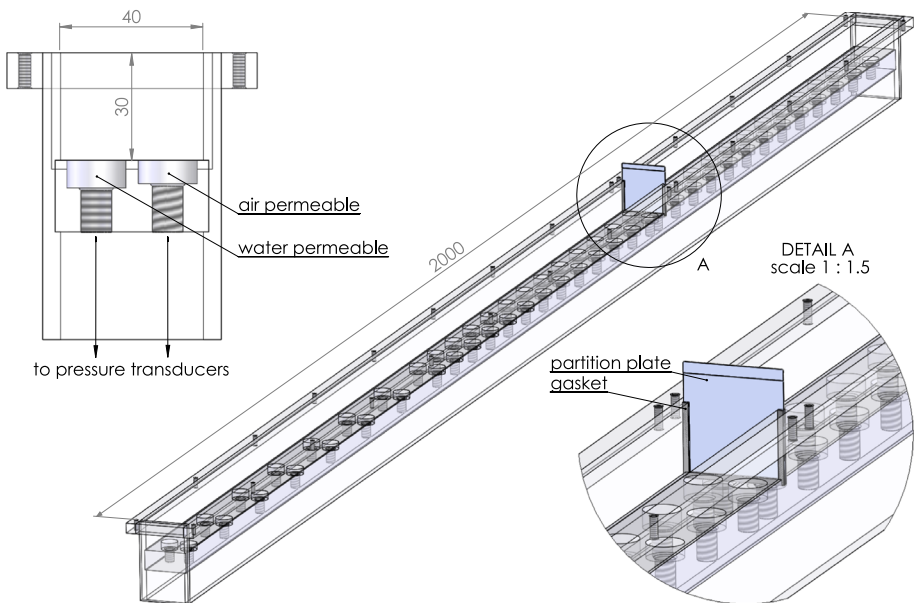
3 Materials and Methods

3.1 The Setup

The idea of the experiment is simple; we wish to observe the horizontal redistribution process in a porous medium with an initial saturation discontinuity. Therefore, a horizontal flume containing a homogeneous sandy soil is constructed. The flume is divided into two parts using a thin removable plate. The two parts contain the same sand packing but at two different uniform water saturations. The experiment is started by removing the thin plate separating the two compartments. Water saturation and both air and water pressures are measured at various points along the flume as a function of time. Water saturations are measured using a movable gamma ray attenuation system. Pressures of air and water are monitored with hydrophobic and hydrophilic tensiometers connected to pressure transducers. Figure 1 shows the realization of the setup at the Research Facility for Subsurface Remediation (VEGAS) at the University of Stuttgart.

3.2 The Flume

A schematic view of the flume is given in Fig. 2. The flume is made of Plexiglas with the following dimensions in milimeter: $2,000 \times 30 \times 40$ ($l \times h \times w$). The width is dimensioned

Fig. 1 The Redistribution Experiment at VEGAS

Fig. 2 Dimensions of the flume, Detail A: Partition plate

based on the following considerations. The accuracy of the gamma measurement strongly depends on the travel distance through the porous medium. A width chosen too large or too small would lead to a bad resolution in saturation measurement. The height of the flume is chosen small enough to allow neglecting the influence of gravity on the process. The flume

contains a notch dividing it in two compartments of 65 and 135 cm length. The compartment of the initial wetter sand is chosen larger as the draining process is expected to have a larger extension due to the higher mobility of water. Philip (1991) suggests even larger ratios of 5–10. A very thin metal sheet (0.044 mm thick) can be inserted in the notch and sealed using silicone gel to block any possible leakage of water prior to the start of the experiment. Each compartment can be closed separately by a lid made of Plexiglas of 1 cm thickness fixed with screws. A layer of hydrophobic rubber of 0.2 cm thickness is used to prevent preferential flow along the lid.

Redistribution of fluids between the two compartments starts as soon as the metal sheet is removed. The metal sheet is treated with an agent that reduces the adhesion of silicone gel to the sheet. This way, less force is required to remove it and it also ensures that the silicone gel will stay behind in the notch, preventing a larger vacant space to be created around the interface.

3.3 Sand Packing

Once the flume is ready for use, it is filled with sand. The sand is manually packed using a wooden frame placed on the top of the flume and compacted by a wooden block fitting almost exactly into the width and the length of each compartment. The preparation of the sand and especially the packing of the flume have to be done very conscientiously because their properties define the quality of the initial conditions. A uniform distribution of the saturation is as important as the uniformity of the packing density along the flume for the formation of a well-defined saturation discontinuity at the interface. The sand used has a maximum grain size of 2 mm, a median grain size d_{50} of 0.275 mm, and a uniformity index d_{60}/d_{10} of 2.19. The grain density ρ_g is 2,546 kg/m^3 and for the preparation of the packing, a bulk density ρ_P of 1,650 kg/m^3 is assumed. The required masses of sand and water are calculated with the given parameters, determined gravimetrically and then mixed in a bucket using a kitchen mixer prior the experiment.

After the disassembly of the flume, the sand was cored in segments of 5 cm length and dried to specify the assumptions. For determining the exact distance of one segment, a measuring tape was fixed on the opened flume. Then metal plates with the exact width of the flume and a thickness of 1 mm were pushed into the sand and limited the segment. The hydraulic conductivity K of a completely saturated sample of the sand was measured in a constant head permeameter to be 6.38E-04 m/s.

3.4 Measurement Devices

3.4.1 Saturation Measurement

Saturation of water in the flume was measured in situ using a gamma radiation system. This is based on the absorption of gamma-radiation through matter according to the Law of Bouguer–Lambert–Beer (Gerthsen et al. 1992). The gamma-system consists of movable, pc-controlled gamma source, and a gamma detection unit. The gamma detection unit consists of a scintillator and a photomultiplier and turns incoming ionizing radiation into a current pulse. These pulses are counted every second and are displayed as a count rate. A density meter, already calibrated with aluminum blocks of known thickness, converts the measured attenuation into the thickness of a fictive aluminum block, which would cause the measured attenuation. A Pt100 sensor installed near the detection unit measures temperature during the experiment (Fig. 9).

Table 1 Measuring positions of the gamma-system in (cm)

Dry side	−44.4	−40.4	−35.4	−29.4	−23.4	−17.4
	−11.4	−5.4	−4.4	−3.4	−2.4	−1.4
Wet side	1.1	2.1	3.1	4.1	5.1	7.1
	9.1	11.1	13.1	19.1	25.1	31.1
	37.1	43.1	49.1	55.1	61.1	67.1
	73.1	79.1	85.1	90.6		

The flume is placed between the source and detection unit. The attenuation of radiation caused by the flume walls, the containing sand, and the water can be measured at 34 defined measuring points (see Table 1) and is given as thickness of an aluminum block.

For determining the attenuation caused by the water and with this the water saturation of the sand the following steps have to be done:

(1) The part of the attenuation caused by the water in the flume has to be determined. This is done after the experiment. The flume is disassembled in segments of 5 cm, and the porosity and the water saturation of the segments are gravimetrically determined. With the porosity, the water saturation and the inner width of the flume, the thickness of the pure water layer in every segment can be calculated (Eq. 7):

$$d_{\mathrm{w}} = d_{\mathrm{i,Flume}} \varphi S_{\mathrm{w}} \mapsto d_{\mathrm{w,Al}} = d_{\mathrm{w}} \frac{\epsilon_{\mathrm{w}}}{\epsilon_{\mathrm{Al}}} \tag{7}$$

with $d_{\mathrm{i,Flume}}$ the inner thickness of the flume and $d_{\mathrm{w,Al}}$ the thickness of water expressed as a thickness of a corresponding aluminum block. As the measured attenuation is given as a thickness of an aluminum block, the determined thickness of the water layer is converted into a thickness of an aluminum block causing the same attenuation. This can be done by knowing the ratio of the absorption coefficients of aluminum ϵ_{Al} and water ϵ_{w} (Färber 1997).

(2) The attenuation of the flume walls and the containing sand has to be determined. Knowing the calculated attenuation of the water from the disassembly and the attenuation measured shortly before the disassembly, the attenuation caused by the flume walls and the containing water can be calculated by subtracting the values. This is done for every segment.

(3) The attenuation caused by water has to be determined for every measuring point. This is reached by subtracting the attenuation of the flume walls and the containing sand from the measured attenuation of each measuring point at each time step.

(4) The attenuation caused by water given in thickness of a corresponding aluminum block has to be converted into water saturation. Knowing the ratio of the absorption coefficients of aluminum ϵ_{Al} and water ϵ_{w}, the thickness of the water layer, the porosity and the inner width of the flume at every measuring point, the water saturation can be calculated (Eq. 8):

$$S_{\mathrm{w}} = \frac{\frac{\epsilon_{\mathrm{Al}}}{\epsilon_{\mathrm{w}}} d_{\mathrm{Al}}}{d_{\mathrm{i,Flume}} \varphi} \tag{8}$$

3.4.2 Pressure Measurement

The pressures of air and water in the flume are measured with 12 sets of tensiometers installed along the flume. Each set consists of two transducers, one made of hydrophilic ceramic and the

other made of hydrophobic Teflon, measuring water, and air pressures, respectively. Transducers have a measuring range of ± 300 mbar and an accuracy of 0.2 mbar. Each transducer exhibits an entry pressure of approximately 500 mbar for the other phase. The transducers are connected by flexible tubes to porous plates glued into the bottom of the flume. By measuring the pressures of air and water at the same horizontal positions, the capillary pressure at that position can be determined. During the experiments, it was shown that the variations in the air pressure with average values from 0.1 to 0.3 mbar at the different measuring points are relatively small compared to the water pressure. For this reason, only the measurement of the water pressures is shown.

3.5 Conducting the Experiments

Before the start of the redistribution experiments, initial conditions for saturation and pressure have to be established. After the packing of the sand, both saturation and pressure are monitored until the changes are very small. This is taken to be the initial situation. For the start of the redistribution experiment, the partition sheet is removed. Both air and water pressures and the water saturation along the flume are recorded as a function of time. Once these are approximately constant in each subdomain, the experiment is terminated. The flume is disassembled, the sand is cored in segments and gravimetrically analyzed to verify the initial packing density and to back-calculate the saturation of each measuring point.

4 Results and Discussion

4.1 Saturation Profiles Along the Flume

Note that in the following figures, positions of points on the imbibing subdomain are shown to have negative values. In order to investigate the redistribution of water in the flume and the fate of the saturation discontinuity at the drainage-imbibition interface, profiles of saturation along the flume at various times are given and discussed in this section. In addition, the gravimetrically examined saturation is shown along with the packing density.

As it can be seen from Fig. 3, the heterogeneity of the packing density along the flume led to saturation variations on both draining and imbibing sides. However, the saturation discontinuity at the drainage-imbibition interface is well defined. Focusing on each side, the heterogeneity makes it difficult to conduct similar experiments providing identical initial conditions, nevertheless the different propagation behaviors become obvious.

As shown in Fig. 4, the imbibing subdomain is characterized by a large increase of the saturation near the interface immediately after the start of the experiment. At the same time, in the draining subdomain, a slight decrease of saturation occurs up to a horizontal position of about 50 cm from the discontinuity. This effect is caused by the higher mobility of water in the wet soil. After 7 days, in the draining subdomain, saturation change reaches the distance of 70 cm, whereas in the imbibing domain, saturation has not increased at positions further than 30 cm from the discontinuity. Even after 30 days, at the end of the measuring area, only a small increase can be observed. As expected, the saturation discontinuity at the drainage-imbibition interface persists even 30 days after the start of experiment. But contrary to expectations, the final saturation gradient on the imbibing side is even steeper than the initial value.
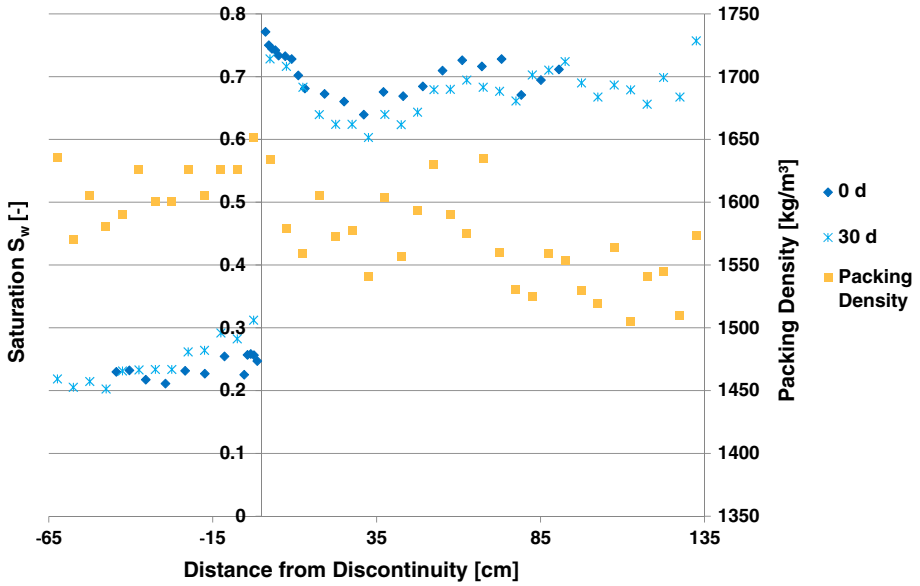
Fig. 3 Initial (0 d) and final (30 d) water saturation profile with packing density along the flume
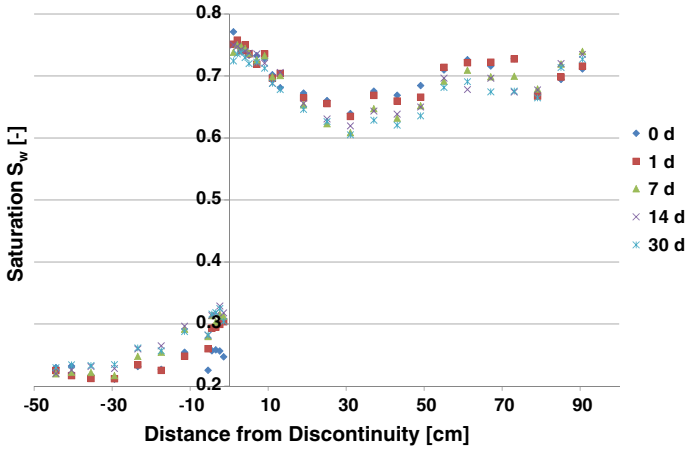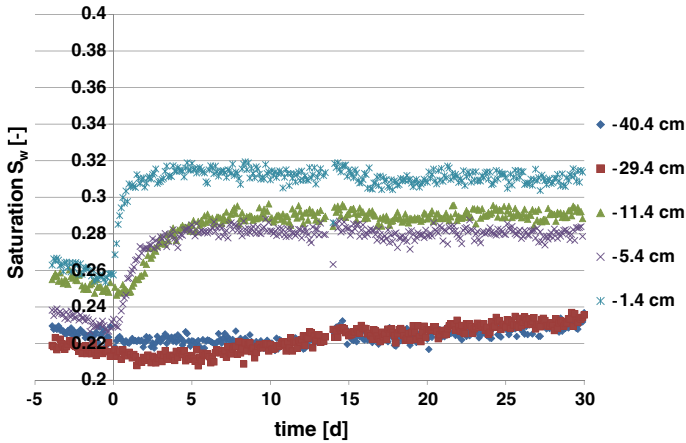

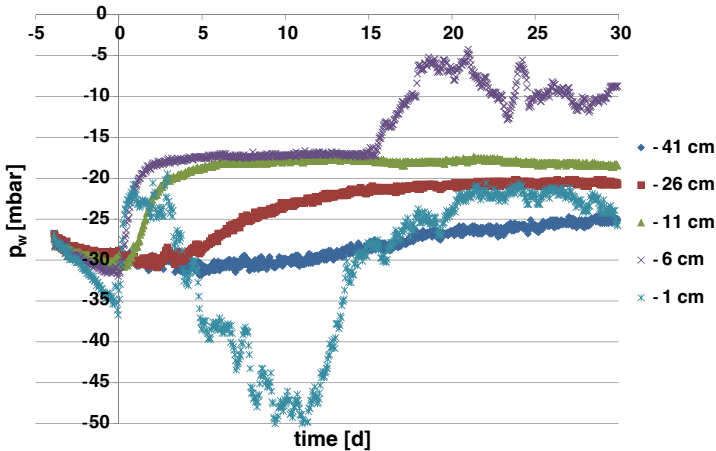**Fig. 4** Temporal development of water saturation profiles along the flume (day 0 through 30)

4.2 Variations in Pressure and Saturation

In this section, the temporal development of the saturation and the corresponding water pressure are shown and analyzed. Due to the high mobility of the air phase, its pressure was found to remain constant in both time and space for the duration of the experiment. Its value remained close to the atmospheric pressure (Fig. 9).

Figure 5 confirms the fast, but horizontally limited, saturation increase on the imbibing side. At positions -1.1 and -5.4 cm from the interface, the saturation increases from 0.26

Fig. 5 Variation of water saturation with time at various locations on the imbibing side

Fig. 6 Variation of water pressure with time at various locations on the imbibing side. The transducers at -1 and -6 cm malfunctioned

and 0.23 to 0.31 and 0.26, respectively, in less than 24 h. At the position -40.4 cm from the interface, a small increase is observable only 11 days after the start of the experiment.

The development of the water pressure on the imbibing side (see Fig. 6) shows a similar behavior with a large and fast change near the interface and a slow and small change at more distant positions. The pressures at the end of the experiment are different in space, but do not seem to be completely constant in time yet. Nevertheless, it is clear that the pressures approach distinctly different values. The pressure transducers at positions -1 and -6 cm seem to have malfunctioned. A reason could be gas bubbles released from the water in the tubes connecting the tensiometer to the transducer. Nevertheless, the pressure measured at position -6 cm already seemed to be constant until it started malfunctioning at day 15 of the experiment. At the end of the experiment, saturations at different positions seem to be constant in time while at different values.
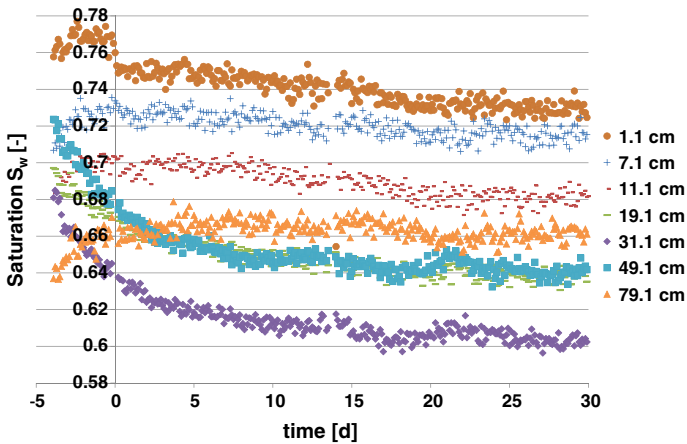
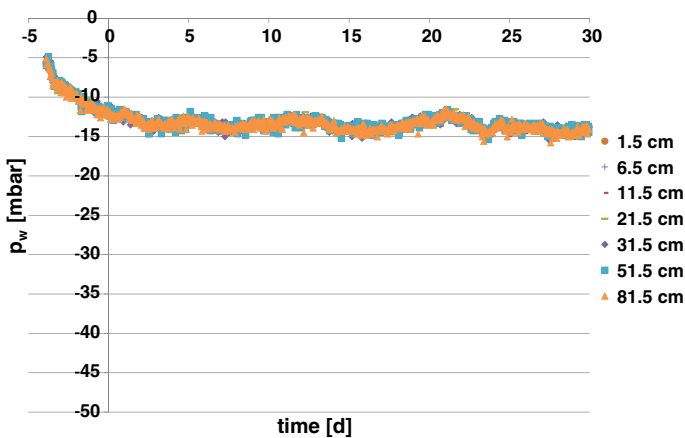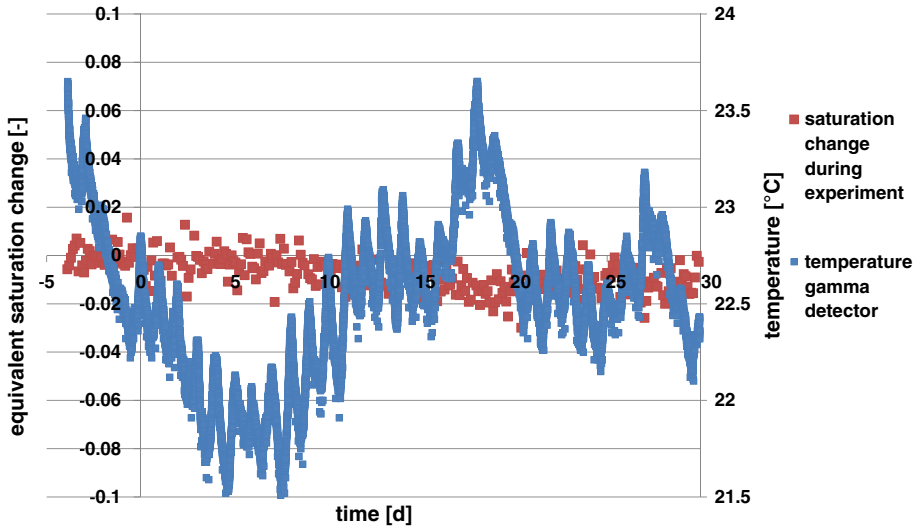**Fig. 7** Variation of water saturation with time at various locations on the draining side

Fig. 8 Variation of water pressure with time at various locations on the draining side

It is important to note that before the start of the redistribution, (data before time zero in Fig. 6), there is no pressure gradient, as there was no flow. Yet at the end of the experiment, even though there is no flow, a pressure gradient clearly persists. This cannot be explained by classical Darcy's Law (Eq. 2), but it is in line with the thermodynamically based approach (Eqs. 5 and 6).

On the draining side (see Fig. 7) a slight, but more extended saturation decrease is obvious. The water pressures measured at transducers in the draining subdomain (see Fig. 8) are the same and become constant shortly after the start of the experiment.

5 Summary and Conclusions

In this work, an experimental setup for investigating horizontal redistribution of two fluid phases with an initial saturation discontinuity was developed and tested. The aim of this work

Fig. 9 Temperature at the gamma-detector

was twofold: (1) to investigate whether a saturation discontinuity will persist as predicted by hysteretic capillarity models, as well as thermodynamically based models and (2) to investigate the long-term behavior of the system, when there is no measurable saturation change and flow. Although equilibrium was not completely reached in the experiment, clear trends can be observed that allow us to answer both points.

Concerning our first focal point, we found experimentally that indeed, a saturation discontinuity persists at the drainage-imbibition interface. With respect to the second issue, our experimental results suggest that even after a long time (30 days) when the system has (almost) come to rest, both a pressure and saturation gradient persist. A saturation gradient on both draining and imbibing sides existed prior the start of the experiment caused by the difficulties of a homogeneous horizontal sand packing. However, the final saturation gradient was even steeper.

This is a hint that the classical Darcy's law does not adequately model two-phase flow. A more complete formulation of Darcy's Law should include gradients of saturation, as well as pressure. These gradients may persist but balance each other under no flow conditions. Further work needs to be done to verify the effects we found for different media, to look at even longer experimental runs, and to quantify the material coefficients related to additional driving forces.

References

Darcy, H.: Détermination des lois d'écoulement de l'eau à travers le sable. Pages 590–594 of: Les Fontaines Publiques de la Ville de Dijon. Victor Dalmont, Paris (1856)

Färber, A.: Wärmetransport in der ungesättigten Bodenzone: Entwicklung einer thermischen In-situ-Sanierungstechnologie. Ph.D. thesis, Universität Stuttgart (1997)

Gerthsen, C., Kneser, H.O., Vogel, H.: Physik. Springer, New York (1992)

Hassanizadeh, S.M., Gray, W.G.: Mechanics and thermodynamics of multiphase flow in porous media including interphase boundaries. Adv. Water Resour. **13**(4), 169–186 (1990)

Hassanizadeh, S.M., Gray, W.G.: Thermodynamic basis of capillary pressure in porous media. Water Resour. Res. **29**(10), 3389–3405 (1993a)

Hassanizadeh, S.M., Gray, W.G.: Toward an improved description of the physics of two-phase flow. Adv. Water Resour. **16**(1), 53–67 (1993b)

Helmig, R.: Multiphase Flow and Transport Processes in the Subsurface. Springer, Berlin (1997)

Joekar-Niasar, V., Hassanizadeh, S.M., Leijnse, A.: Insights into the relationship among capillary pressure, saturation, interfacial area and relative permeability using pore-scale network modeling. Transp. Porous Media **74**, 201–219 (2008)

Marshall, F.: Numerical solution of Philip's redistribution problem. Dipl.-Ing. thesis, Institute of Hydraulic Engineering, University of Stuttgart (2009)

Philip, J.R.: Horizontal redistribution with capillary hysteresis. Water Resour. Res. **27**, 1459–1469 (1991)

Pop, I.S., van Duijn, C.J., Niessner, J., Hassanizadeh, S.M.: Horizontal redistribution of fluids in a porous medium: the role of interfacial area in modeling hysteresis. Adv. Water Resour. **32**(3), 383–390 (2009)

Richards, L.A.: Capillary conduction of liquids through porous mediums. Physics **1**, 318–333 (1931)